Reduced scale laboratory physical model for a geotextile reinforced embankment under groundwater flow

Abdullah Tolga Özer & Onur Akay
Department of Civil Engineering, Okan University, Turkey

ABSTRACT: Geotextiles are used as basal reinforcement for the embankments constructed on soft soil sites as an alternative to the conventional soil improvement techniques. The failure scenarios of geotextile reinforced embankments generally involve bearing capacity, global stability, elastic deformation, pullout and lateral spreading analysis. However, the behavior of geotextile reinforced embankments under seepage flow has not been thoroughly investigated since most design guidelines require a proper drainage system to prevent pore water pressure accumulation within the embankment. This study investigates the behavior of an embankment reinforced by nonwoven geotextile in the case of groundwater flow within the embankment. For this purpose, a laboratory model of a geotextile reinforced embankment with the dimensions of 195 cm long, 100 cm wide, and 110 cm high was constructed. Embankment, comprised of well drained sand, with a side slope angle of 45 degrees was constructed in a controlled manner by performing the compaction in 5 cm lifts to form a uniform domain with a dry density of 14.0 kN/m^3. Constant hydraulic head of 100 cm was applied using the water reservoir located behind the model. Vibrating wire pressure cells were used to monitor total pressures during both construction stage and seepage experiment. In addition, pencil size tensiometers and piezometers were used to capture piezometric conditions on the side and within the embankment, respectively. Behavior of the geotextile reinforced embankment under seepage was compared to that of unreinforced (Matrix) embankment under the same hydraulic boundary condition. Due to the limited in-plane drainage capacity (transmissivity), non-woven geotextile reinforcement was not able to alleviate the pore water pressures within the embankment. Therefore, as in the case of Matrix embankment, deep-seated global stability failure starting from the crest and exiting at the toe of the embankment was occurred.

Keywords: Drainage, Geotextile Reinforced Embankment, Seepage, Slope stability

1 INTRODUCTION

Geotextiles are used as basal reinforcement to improve the stability of embankments (geotextile reinforced embankments) constructed on weak subsurface profiles (Fowler and Edris, 1987; Voskamp and Risseeuw, 1987; Rowe and Gnanendran, 1994; Palmeria et al., 1998; Rowe and Li, 2005). Geotextiles not only allow uniform stress distributions at the base of the embankment, but also prevent potential lateral spreading of the embankment over the poor foundation conditions (Christopher and Wagner, 1988). In addition, geotextile basal reinforcement reduces foundation settlement (Zhang et al., 2015) and also increases embankment failure heights (Bergado et al., 1994; Rowe and Soderman, 1987; Rowe and Li, 2005). Furthermore, geotextile basal reinforcement offers more economical solution when compared with the conventional techniques (Rowe and Li, 2005).

While, geotextiles are generally used as a filtration material as an alternative to granular soil filters (Veylon et al., 2016), their drainage capacities are limited when compared to that of geocomposite drains (Koerner, 2012). Constructing embankments over soft soil sites using geotextile basal reinforcement has been extensively studied and well proven technique by utilizing the reinforcement function of geotextiles.

However, there are limited studies on drainage behaviors of geotextiles used as reinforcement (Tan et al., 2001).

The failure scenarios of a basal geotextile reinforced embankments constructed on soft soil sites can be listed as; bearing capacity, global stability, elastic deformation, pullout or anchorage and lateral spreading (Koerner et al., 1987). There are several numerical solutions that have been used for those stability analyses (Palmeria et al., 1998; Bergado et al., 2002; Borges and Cardoso, 2002; Hinchberger and Rowe, 2003; Wulandari and Tjandra, 2015; Smith and Tatari, 2016). While the failure scenarios are all considering the mechanical properties of geotextile (Koerner et al., 1987), the failure scenario of geotextile reinforced embankments under seepage were not considered.

The behavior of the nonwoven geotextile reinforced granular slopes under infiltration and their contribution as a drainage medium has been investigated by Iryo and Rowe (2005). They concluded that contribution of nonwoven geotextiles to the stability as a drainage material is much limited when compared to that of reinforcement function. However, Tan et al. (2001) has demonstrated that geotextile reinforcement effectively alleviated excess pore water pressures under external loading in poorly drained residual soil.

Well graded granular materials are preferred to construct geosynthetic reinforced earth structures to meet the stress transfer, soil-reinforcement interaction, drainage and constructability requirements (Mitchell and Villet, 1987; Berg et al., 2009). In addition, the Federal Highway Administration (FHWA) current specification requires granular fill material with a maximum plastic index of 6, maximum particles passing 200 sieve to be less than 15% and the maximum grain size of 19 mm for reinforced embankments using geosynthetics (Wahls, 1990). In this study, the behavior of geotextile reinforced embankment (constructed from material which conforms to the FHWA requirement) was studied in the case of groundwater flow within the embankment. The behavior of geotextile reinforced embankment was compared with the unreinforced embankment of Akay et al. (2016) under the same hydraulic condition (matrix embankment).

2 MATERIALS AND METHODS

Reduced scale laboratory embankment models were constructed in 200 cm long, 100 cm wide and 220 cm high Plexiglas test bed (Elbeyli, 2016; Pusar, 2016; Akay et al., 2016; 2017) which is supported by steel frame (Figure 1a, b). The constant hydraulic head of 100 cm-H_2O was provided by a water compartment, located behind the model (Figure 1). A Plexiglas perforated panel with 8 mm holes allowed water to infiltrate into the soil compartment in which embankment models were constructed. A steel mesh filter with an opening size of 0.063 mm was placed on the soil compartment side of the perforated separation panel to prevent soil entry to the water compartment. Both matrix and geotextile reinforced embankments were constructed with the dimensions of 195 cm long, 100 cm wide, and 110 cm high (Figure 1c). Embankments with a side slope of 45 degrees (1 Vertical:1 Horizontal) were constructed by controlled compaction in 5 cm lifts (Figure 2) to form a slope of 14 kN/m^3.

A total of 13 pencil size tensiometers (T1-T13) coupled with pressure transducers (Figure 1c) were installed at one side of the test bed to record pore-water pressures developed near the wall of the test bed. In addition, embankment models were equipped with a total of 5 vibrating wire pressure cells (TP1-TP5, Figure 2a) to capture total pressures in the matrix embankment. Total pressure cells were installed at the top of nonwoven geotextile, placed on the first lift (Figure 2b). A total of 3 piezometers (P1-P3, Figures 2c, d, e) to record the pore water pressures within the slope. Location of these tensiometers, piezometers and total pressure cells (x, y, z) were listed based on to the reference point (0, 0, 0) located at the lower left corner of the model (Figures 1c and 2).

The physical, mechanical and hydraulic properties of the poorly-graded sand used to construct the physical slope models is studied by Pusar (2017) and summarized in Table 1. Grain size distribution (ASTM D6913) properties, maximum and minimum void ratios (ASTM D4253 and ASTM D 4354), specific gravity (ASTM D854) results summarized in Table 1 are the average values of a total of six tests. Average strength parameters presented in Table 1 is the average of a total of three consolidated drained (CD) triaxial test (ASTM D7181) results. The average saturated hydraulic conductivity value is based on a total of six constant head hydraulic conductivity (ASTM D2434) tests. The properties of nonwoven geotextile are also listed in Table 1.

Figure 1. Laboratory test bed (a) Plexiglas test bed with steel frame (a) Plexiglas test bed with steel frame, alternative view (c) Embankment model and location of tensiometers (Akay et al., 2017).

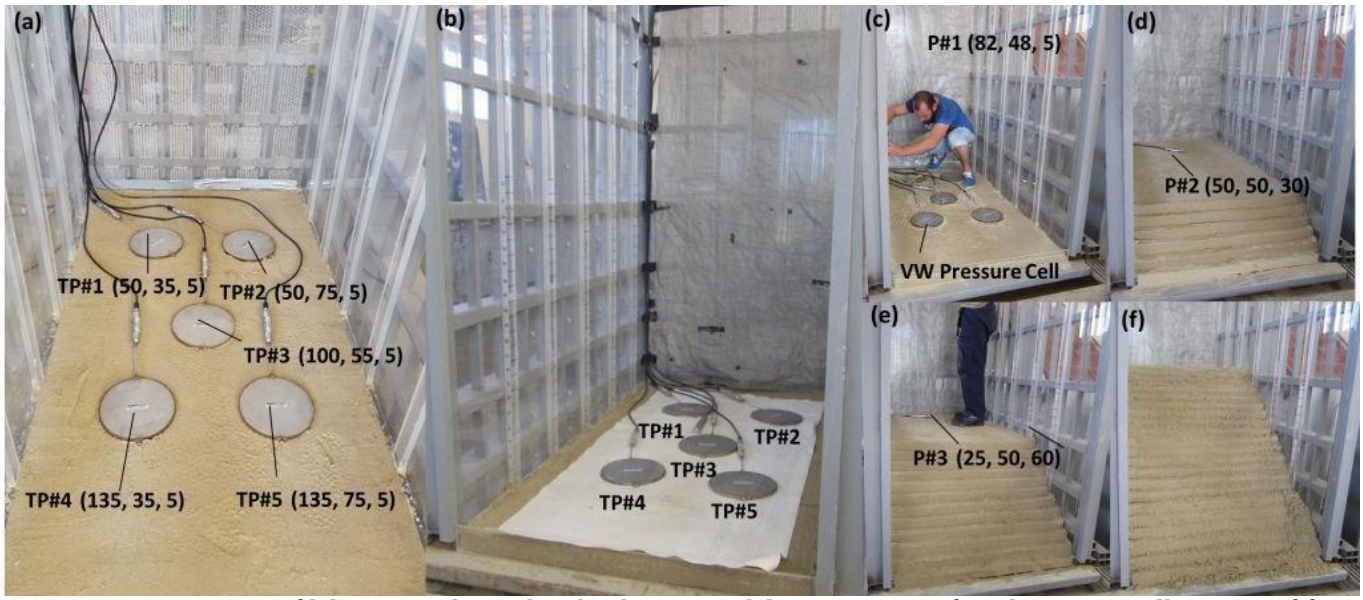

Figure 2. Construction of laboratory physical embankment model (a) Location of total pressure cells on top of first lift, h = 5 cm, matrix embankment (b) Location of total pressure cells on top of nonwoven geotextile, h = 5 cm, geotextile reinforced embankment (c) P#1 located at the first lift, h = 5 cm (d) P#2 located at the 6th lift, h = 30 cm (e) P#3 located at the 12th lift, h = 60 cm (e) 22nd lift, completed slope, h = 110 cm.

Table 1. Properties of poorly graded sand and nonwoven geotextile.

Property		Description and Unit	Value
Material: Sand			
Material Classification		Unified soil classification system	SP
Effective Size		D_{10} (mm)	0.15
Uniformity Coefficient		C_u [-]	2.8
Coefficient of Curvature		C_c [-]	1.5
Specific Gravity		Gs [-]	2.62
Maximum Void Ratio		e_{max} [-]	0.93
Minimum Void Ratio		e_{min} [-]	0.62
Effective Shear Strength Parameters	Cohesion	c' [kPa]	0
	Internal Friction Angle	ø' [degrees]	31.8
Saturated Hydraulic Conductivity		k_{sat} [m/s]	$1.1x10^{-4}$
Material: Nonwoven Geotextile			
Polymer Type		[-]	Polypropylene
Mass Per Unit Area		[gr/m^2]	120
CBR Puncture Strength		[kN]	1.4
Flux Perpendicular to the Plane		[l/m^2s]	90
Apparent Opening Size		AOS [µm]	<170

3 RESULTS AND DISCUSSIONS

The construction of the matrix embankment model was started on 18.08.2015 and completed on 25.08.2015 (Figure 3a), and the construction on the geotextile reinforced embankment was started on 11.03.2016 and completed on 15.03.2016 (Figure 3b). Estimated total pressures during the stage construction of the reduced scale embankment models were compared with working stresses captured by TP#1 and TP#2. In both reduced scale models, the magnitude of working stresses followed the estimated loading history (Figure 3). The decreasing trend in between the end of construction and the beginning of the test is attributed to the settlement of fist lift (h = 5 cm) where total pressure cells were installed (Figure 3).

The physical condition of the matrix embankment at the end of the test is shown in Figure 4. A deep-seated failure entering from the crest and exiting at the toe was occurred and the failure surface (hypothesized rotational failure plane) indicated by a dash-line in Figure 4 (Akay et al., 2016).

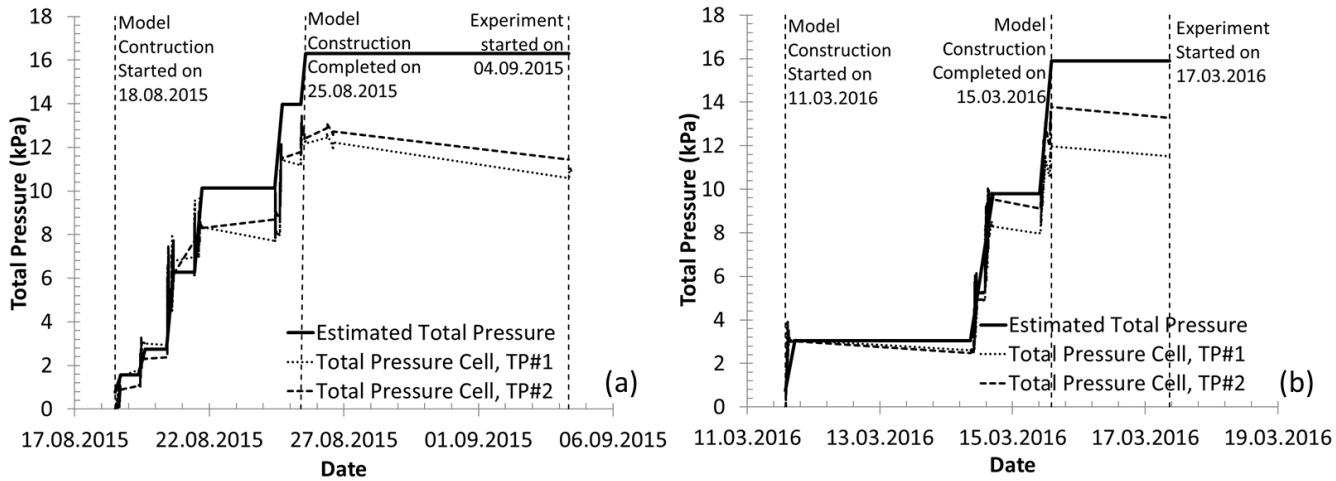

Figure 3. Comparison of estimated and working stress conditions during construction of the reduced scale laboratory embankment model (a) Matrix configuration (b) Embankment reinforced with nonwoven geotextile

Pore-water pressure recordings obtained by tensiometers T4, T8, T11 and T13 (tensiometers located along the bottom of the model, Figure 1) during the test are presented in Figure 5a. Time of seepage, which represents the seepage emergence at the toe of the slope, and global failure initiation time, which represents the failure initiation under seepage forces were recorded (Figure 5). Pore-water pressure time series obtained by piezometers were presented in Figure 6a. Test was terminated when the steady-state soil-pore water pressure recordings were well established.

Figure 4. Physical condition of the matrix embankment at the end of the test (a) Side view of the failure surface with hypothesized rotational failure plane entering at the crest and exiting at the toe (b) Front view of the failure surface (Akay et al., 2016)

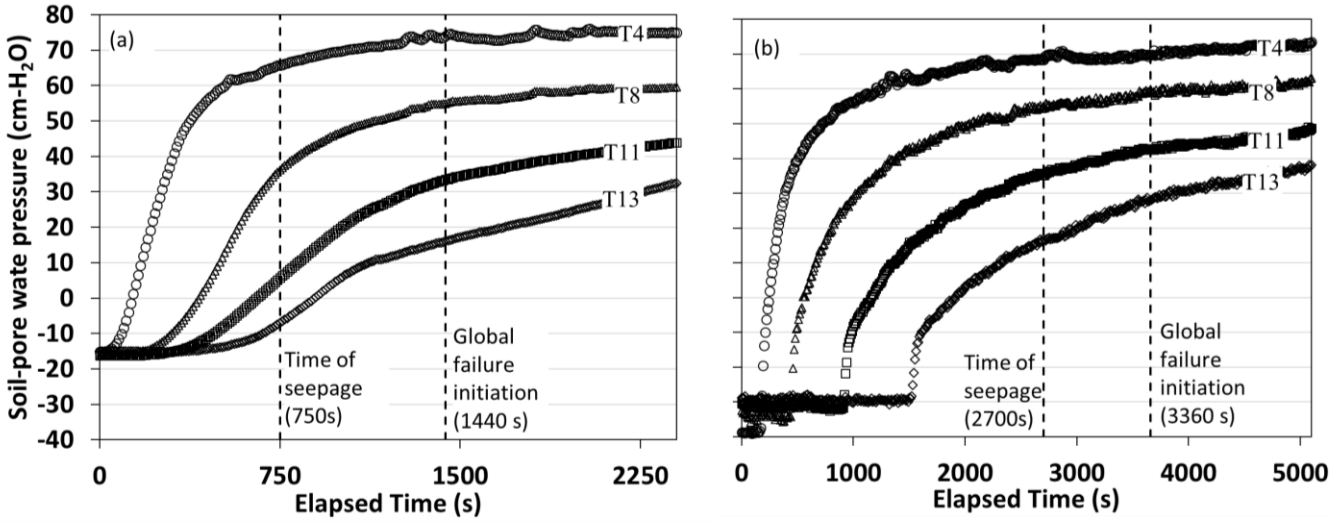

Figure 5. Pore-water pressures recorded by tensiometers under 100 cm-H_2O boundary condition (a) Matrix configuration (b) Embankment reinforced with nonwoven geotextile

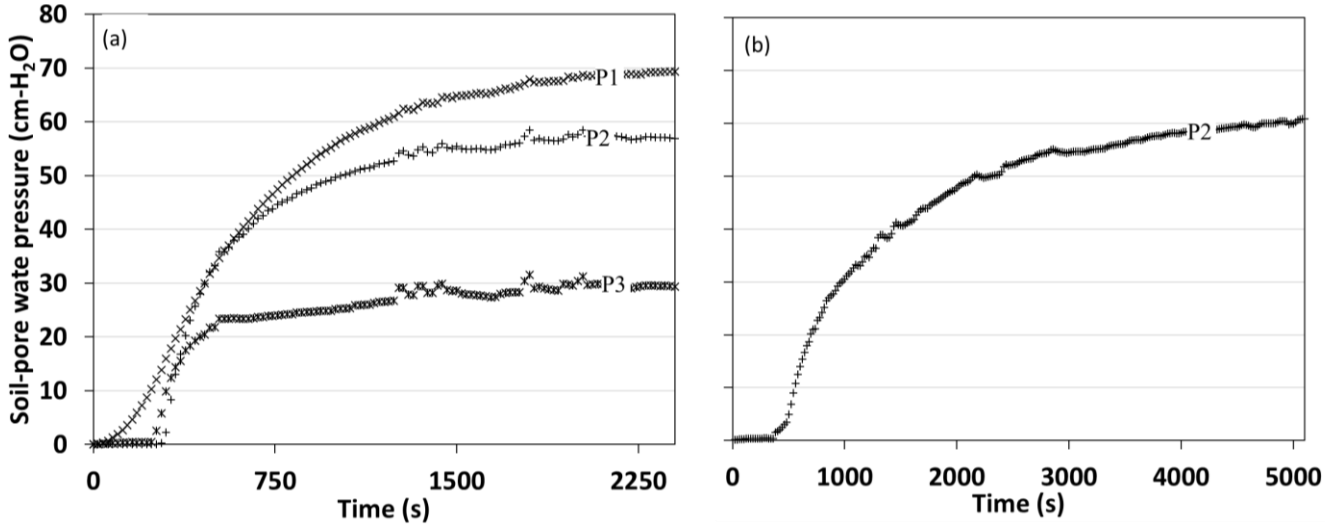

Figure 6. Pore-water pressures recorded by piezometers under 100 cm-H_2O boundary condition (a) Matrix configuration (b) Embankment reinforced with nonwoven geotextile

The physical condition of the geotextile reinforced embankment during the test was shown in Figure 7. Seepage exit was observed at the toe 45 min after the test has started (Figure 7a). Upon initiation of the seepage at the toe, the physical slope deformations have started (Figure 7b). These small deformations progressed as shallow-seated failures. These shallow-seated failures reached a state where they trigger the global failure (global failure initiation time, Figure 7c). Shortly after, failure plane entrance moved all the way up to the crest and a deep-seated failure occurred (Figure 7d). Similar to that of matrix embankment (Figure 4), a deep-seated failure surface entering from the crest and exiting at the toe (hypothesized rotational failure plane) was indicated by a dash-line in Figure 7e.

Pore-water pressure time series obtained by both tensiometers (T4, T8, T11 and T13) and a piezometer (P2) are presented in Figures 5b and 6b, respectively. Time of seepage and global failure initiation time were also recorded (Figure 5). Test was terminated when the steady-state soil-pore water pressure recordings were well established.

In both experiments, soil pore water pressures were gradually increased until time of seepage and continued to rise with a much slower rate until global failure initiation (Figures 5 and 6). After global failure initiation, steady state flow conditions were established in both T4 and T8 (Figure 5). However, pore-water pressure responses captured by the tensiometers near the toe, T8 and T11, indicated a gradual increase after global failure initiation (Figure 5). This increase in these tensiometers was attributed to soil accumulation near the toe due to global failure of the embankments under seepage forces.

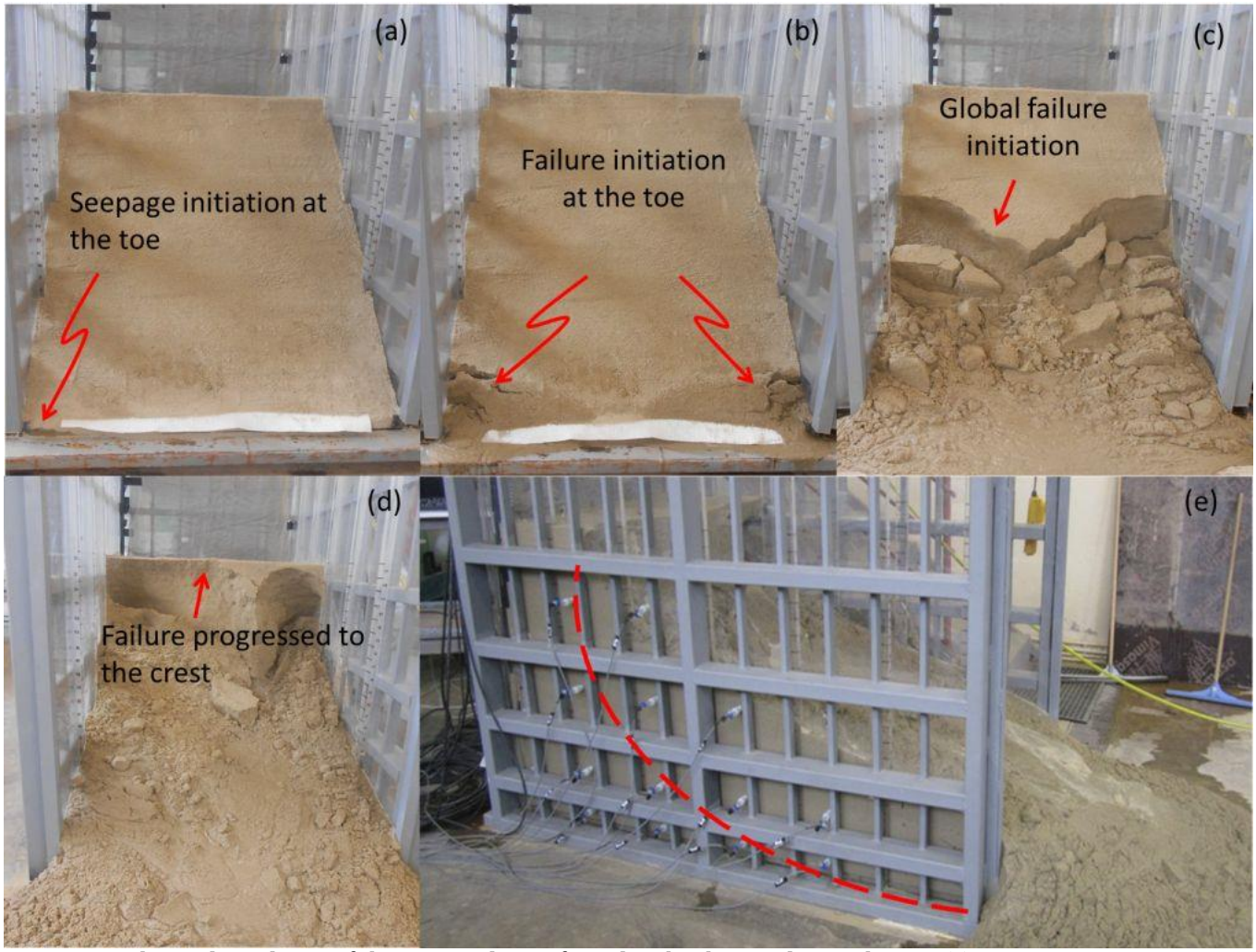

Figure 7. Physical condition of the geotextile reinforced embankment during the test (a) Seepage initiation t = 45 min (b) Failure initiation at the toe observed at t = 50 min (c) Global failure initiation has started at t = 56 min (d) Failure progressed at the crest at t = 70 min (e) At the end of the test, t = 85 min

The global failures observed in both matrix and geotextile reinforced slopes (Figures 4b and 7e, respectively) can be explained by the limited in-plane drainage capacity of nonwoven geotextile which could not alleviate the pore-water pressures within the embankment (Figures 5 and 6). Pore-water pressure response in both matrix and geotextile reinforced embankments were similar (Figure 5 and 6). At the steady state, soil-pore pressure responses captured by tensiometers T4, T8, T11 and T13 in geotextile reinforced embankment were 73.5 cm-, 62.5 cm, 48.5 cm- and 37.7 cm-H_2O, respectively (Figure 5b).

Soil-pore pressure recordings in matrix embankment by tensiometers T4, T8, T11 and T13 were 75 cm-, 59.5 cm, 44.0 cm- and 32.5 cm-H_2O, respectively (Figure 5a). These similarities were also observed in piezometers. Pore-water pressures recorded by P2 were 57.2 cm- and 59.9 cm-H_2O for matrix embankment and geotextile reinforced embankment, respectively (Figure 6).

The comparison of the pore-water pressures measured within the slope by piezometers and near the wall by tensiometers was shown in Figure 8. At the steady state, Piezometer P3 measured a pore-water pressure of 29.3 cm-H_2O and tensiometer T2 measured 31.6 cm-H_2O in the matrix embankment (Figure 8a). At the steady state, Piezometer P2 measured a pore-water pressure of 60.0 cm-H_2O and tensiometer T7 measured 54.0 cm-H_2O in the geotextile reinforced embankment (Figure 8b). These similar responses by the tensiometers and piezometers indicated that groundwater flow was homogeneous and not affected by the walls of the Plexiglas test bed.

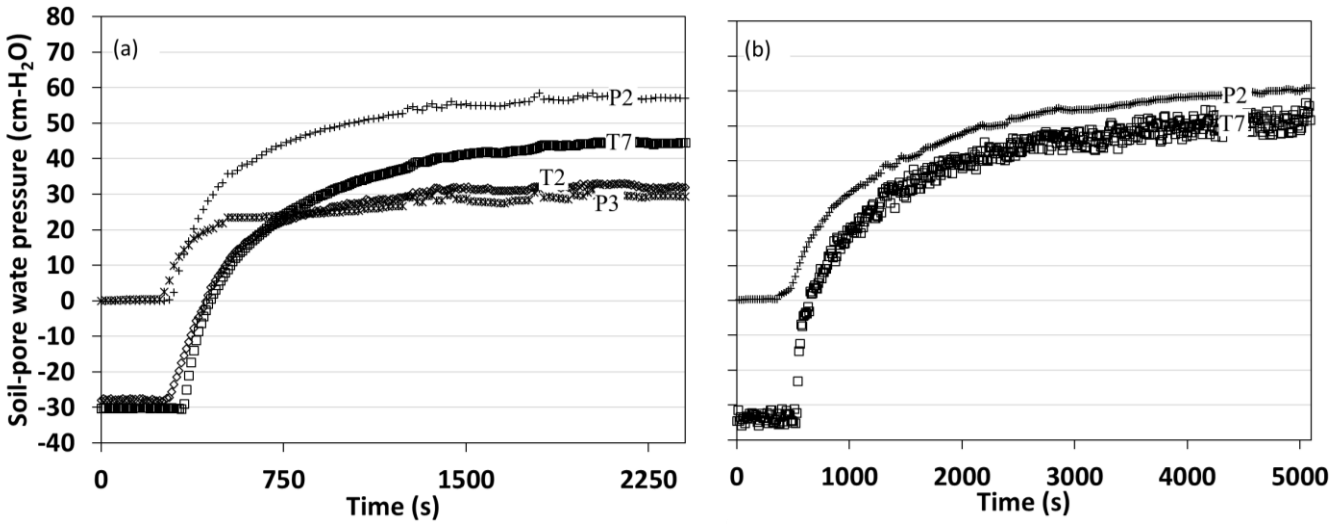

Figure 8. Comparison of measured pore-water pressures recorded by tensiometers and piezometers (a) Matrix configuration (b) Embankment reinforced with nonwoven geotextile

4 CONCLUSIONS

Behavior of the geotextile reinforced embankment under seepage was compared with matrix embankment under the same hydraulic boundary condition. Similar pore-water pressures were observed in both matrix and geotextile reinforced slopes under seepage. Geotextile was not able to alleviate the pore-water pressures within the embankment due to its limited in-plane drainage capacity. As a result, a deep-seated global stability failure was occurred in geotextile reinforced embankment similar to that of matrix embankment.

Geotextile basal reinforcement is traditionally preferred constructing embankments on soft soil sites to improve the stability of the embankments, to prevent the potential lateral spreading and reduce the settlement. Besides the all mechanical advantages of the high strength geotextiles, their in-plane flow capacities are very limited. This study concluded that when the geotextiles used as a basal reinforcement for sandy embankments subjected to seepage, additional measures needs to be implemented into the design. The results of this study are based on reduced scale laboratory physical embankment models which can only provide insights into the prototype embankment behaviors.

ACKNOWLEDGEMENTS

The authors acknowledge the contribution of Murat Pusar and Yalçın Elbeyli, former graduate students, and Halis Şahin, laboratory technician at the Okan University Civil Engineering Laboratory, for their efforts during the construction of the physical models.

REFERENCES

Akay, O., Özer, A. T., Yüzer, Y., Bilen, M. & Bozkır, Ş., 2017. Three-dimensional laser scanning for laboratory-scale assessment of seepage erosion. Proceedings of 9th Hydrology Congress, Diyarbakir, Turkey, In Turkish.

Akay, O., Özer, A.T., Elbeyli, Y. & Pusar, M., 2016. Investigating the failure mechanisms of sandy slopes under seepage using reduced scale laboratory models, 4th International Conference on New Developments in Soil Mechanics and Geotechnical Engineering.

Berg, R. R., Christopher, B. R. & Samtani, N. C. 2009. Design of mechanically stabilized earth walls and reinforced soil slopes – volume I, Federal Highway Administration, FHWA, Report No FHWA-NHI-10-024, National Highway Institute, NHI Courses No. 132040 and 132043.

Bergado, D. T., Lorenzo, G. A. & Long, P. V. 2002. Limit equilibrium method back analyses of geotextile-reinforced embankments on soft Bangkok Clay – a case study, Geosynthetics International, 9 (3), pp. 217 – 245.

Bergado, D. T., Long, P. V., Lee, C. H., Loke, K. H. & Werner, G., 1994. Performance of reinforced embankment on soft Bankok Clay with high-strength geotextile reinforcement, Geotextiles and Geomembranes, 13, pp. 403-420.

Borges, J. L. & Cardoso, A. S. 2002. Overall stability of geosynthetic-reinforced embankment on soft soils, Geotextiles and Geomembranes, 20, pp. 395-421.

Christopher, B. R. & Wagner, A. B. 1988. A Geotextile Reinforced Embankment for a Four Lane Divided Highway – U.S. Hwy. 45, West Bend, Wisconsin, International Conference on Case Histories in Geotechnical Engineering, p. 1093-1098.

Elbeyli, Y. 2016. Investigating the behavior of geotextile reinforced sandy embankments under seepage flow by laboratory tests, Master of Science Thesis, Okan University, Istanbul, Tukey, In Turkish.

Fowler, J. & Edris E. V. 1987. Fabric reinforced embankment test section, Geotextiles and Geomembranes, 6, pp.1-31.

Hinchberger, S. D. & Rowe, R. K. 2003. Geosynthetic reinforced embankments on soft clay foundations: predicting reinforcement strains at failure, Geotextiles and Geomembranes, 21, pp. 151-175.

Iryo, T. & Rowe, R. K., 2005. Infiltration into an embankment reinforced by nonwoven geotextiles, Canadian Geotechnical Journal, 42, pp. 1145-1159.

Koerner, R. M. 2012. Designing with geosynthetics, 6th Edition, Xlibris Cooporation.

Koerner, R. M., Hwu, B-L. & Wayne, M. H. 1987. Soft soil stabilization designs using geosynthetics, Geotextiles and Geomembranes, 6, pp. 33-51.

Mitchell, J. K. & Villet, W. C. B. 1987. Reinforcement of earth slopes and embankments, National Cooperative Highway Research Program, NCHRP, Report Number 290, Transportation Research Board, Washington D.C., USA.

Palmeria E. M., Pereira, J. H. F. & da Silva, A. R. L. 1998. Back analyses of geosynthetic reinforced embankments on soft soils, Geotextiles and Geomembranes, 16, pp. 273-292.

Pusar, M. 2017. Investigating the behavior of geotextile and geocomposite drains used at the base of sandy embankments under seepage flow by laboratory tests, Master of Science Thesis, Okan University, Istanbul, Tukey, In Turkish.

Rowe, R. K. & Li, A. L. 2005. Geosynthetic-reinforced embankments over soft foundations, Geosynthetics International, 12 (1), pp. 50-85.

Rowe, R. K. & Gnanendran, C. T. 1994. Geotextile strain in a full scale reinforced test embankment, Geotextiles and Geomembranes, 13, pp. 781-806.

Rowe, R. K. & Soderman, K. L., 1987. Stabilization of very soft soils using high strength geosynthetics: The role of finite element analyses, Geotextiles and Geomembranes, 6, pp. 53-80.

Smith, C.C. & Tatari, A. 2016. Limit analysis of reinforced embankments on soft soil, Geotextiles and Geomembranes, 44, 504-514.

Tan, S. A., Chew, S. H., Ng, C. C., Loh, S. L., Karunaratne, G. P., Delmas, Ph. & Loke, K. H. 2001. Large-scale drainage behavior of composite geotextile and geogrid in residual soil, Geotextiles and Geomembranes, 19, pp. 163-176.

Veylon, G., Stoltz, G., Meriaux, P., Faure, Y-H. & Touze-Foltz, N. 2016. Performance of geotextile filters after 18 years service in drainage trenches, Geotextiles and Geomembranes, 44, pp. 515-533.

Voskamp, W. & Risseeuw, P., 1987. Method to establish the maximum allowable load under working conditions of polyester reinforcing fabrics, Geotextiles and Geomembranes, 6, pp. 173-184.

Wahls, H. E. 1990. Design and construction of bridge approaches, Federal Highway Administration, FHWA, National Cooperative Highway Research Program, NCHRP Report No 159, Trasportation Research Board, TRB, Washington D. C., USA.

Wulandari, P. S. & Tjandra, D. 2015. Analysis of geotextile reinforced road embankment using Plaxis 2D, Procedia Engineering, 125, pp. 358-362.

Zhang, N., Shen, S.L., Wu, H.N., Chai, J.C. & Xu, Y.S. 2015. Evaluation of effect of basal geotextile reinforcement under embankment loading on soft marine deposits, Geotextiles and Geomembranes, 43, pp. 506-514.